

# Hybrid functional study of proper and improper multiferroics

A. Stroppa and S. Picozzi

*Consiglio Nazionale delle Ricerche*

*Istituto Nazionale di Fisica della Materia (CNR-INFM),*

*CASTI Regional Laboratory,*

*67010 L' Aquila, Italy*

## Abstract

We present a detailed study of the structural, electronic, magnetic and ferroelectric properties of prototypical *proper* and *improper* multiferroic (MF) systems such as  $\text{BiFeO}_3$  and orthorhombic  $\text{HoMnO}_3$ , respectively, within density functional theory (DFT) and using the Heyd-Scuseria-Ernzerhof hybrid functional (HSE). By comparing our results with available experimental data as well as with state-of-the-art GW calculations, we show that the HSE formalism is able to account well for the relevant properties of these compounds and it emerges as an accurate tool for predictive first-principles investigations on multiferroic systems. We show that effects beyond local and semilocal DFT approaches (as provided by HSE) are necessary for a realistic description of MFs. For the electric polarization, a decrease is found for MFs with magnetically-induced ferroelectricity, such as  $\text{HoMnO}_3$ , where the calculated polarization changes from  $\sim 6 \mu\text{C}/\text{cm}^2$  using Perdew-Burke-Ernzerhof (PBE) to  $\sim 2 \mu\text{C}/\text{cm}^2$  using HSE. However, for *proper* MFs, such as  $\text{BiFeO}_3$ , the polarization slightly increases upon introduction of exact exchange. Our findings therefore suggest that a general trend for the HSE correction to bare density functional cannot be extracted; rather, a specific investigation has to be carried out on each compound.

PACS numbers: 75.80.+q; 75.47.Lx; 75.50.Ee; 77.80.-e; 71.15.Ap;

## I. INTRODUCTION

Multiferroics (MFs) are materials in which different ferroic orders such as ferromagnetism, ferroelectricity and/or ferroelasticity may coexist in a single compound.[1] They have attracted much attention for their potential applications in memory devices and other electronic components, due to the intriguing possibility of controlling magnetism by an applied electric field, and viceversa (magnetoelectric effect).[2–5]

Multiferroics are compounds where electron correlations are rather important, and where the electron charge shows atomic-like features, such as strong space localization, poorly dispersed band energies, and large on-site Coulomb repulsion.[3, 4, 6, 7] For these systems, there are well-known deficiencies of local-spin-density approximation (LSDA) or spin-polarized generalized-gradient-approximation (SGGA) to density-functional-theory (DFT). Among them, we recall the underestimation of the band-gap magnitude for most insulating materials.[8–10] Part of these failures can be traced back to the self-interaction error in approximate density functionals: the electron charge experiences a spurious interaction with the Coulomb and exchange-correlation potential generated by itself.[11, 12]

The LSDA+ $U$ [13–15] and the self-interaction correction (SIC) schemes[16–18] can overcome some of the deficiencies of LSDA. However, LSDA+ $U$  suffers ambiguities in the choice of the  $U$  parameter and needs a choice regarding which orbitals to treat within a Hubbard-like approach. For simple materials, a self-consistent evaluation of the  $U$  parameter can be obtained, although this method is not widely used.[19] For BiFeO<sub>3</sub>, the value  $U_{eff}=3.8$  eV has been recently calculated.[20]

SIC-schemes are not commonly available in electronic structure codes for extended solid state systems. The implementation of a fully self-consistent SIC-LSDA approach for extended systems was done by Svane and co-workers.[21] Since then, other approaches have been implemented (for a review, see Refs.[17, 22]). SIC-schemes suffer from the “nonvariationality-problem” of the energy functional which makes forces and stress calculation not commonly available.[23]

In the last few years, hybrid Hartree-Fock density functionals[24–27] have been widely used in solid state physics,[27–30] ranging from simple semiconductor systems,[30] to transition metals, lanthanides, actinides,[31–34] molecules at surfaces,[35, 36] diluted magnetic semiconductors,[37] carbon nanostructures.[38, 39] For a recent review see Ref.[40]. Hybrid

functionals mix the exact nonlocal exchange of Hartree-Fock theory[24–27] with the density functional exchange. The Heyd-Scuseria-Ernzerhof screened hybrid functional (HSE)[41, 42] is well suited for extended solid state systems.

There are very few studies dealing with ferroelectric oxides and even less with multiferroics. Wahl *et al.* re-investigated the well-known  $\text{SrTiO}_3$  and  $\text{BaTiO}_3$  [43] using HSE and semilocal functionals (LDA,PBE,[44] PBEsol[96]). Bilc *et al.* studied in great details  $\text{BaTiO}_3$  as well as  $\text{PbTiO}_3$  using the B1-WC hybrid-functional and concluded that the latter gives an accurate description of both the structural and electronic properties.[45] Goffinet *et al.* extended the analysis to the prototypical multiferroic bismuth ferrite showing that hybrid-functionals, specifically the B1-WC functional, open new perspectives for a better first-principles description of multiferroics.[46] In passing, we recall that the WC gradient corrected functional[47] is very similar to PBEsol and the hybrid B1-WC[48] functional mixes the WC functional with 16% nonlocal exchange. The hybrid HSE functional mixes 25% nonlocal exchange with the PBE functional and the mix is performed only on the short range component of the Coulomb interaction (for further details, we refer to Ref. 43). However, which functional to prefer for simple ferroelectric compounds is still an open issue.[43]

So far, a good performance of HSE or B1-WC functionals has been recognized for *proper* multiferroics where the ferroelectric polarization is of displacive type. On the other hand, magnetically driven multiferroics, also known as *improper* multiferroics, are largely unexplored using hybrid functionals. The purpose of this work is to extend the previous hybrid density functional studies from prototypical ferroelectric oxides ( $\text{SrTiO}_3$ ,  $\text{BaTiO}_3$ ,  $\text{PbTiO}_3$ )[43, 45] or simple multiferroic system ( $\text{BiFeO}_3$ ) to more complicated and exotic multiferroic compounds, such as  $\text{HoMnO}_3$ .

First of all, we focus on  $\text{BiFeO}_3$ , already investigated using the B1-WC functional, but not yet using HSE. In this way, we are able to compare two different, although similar, approaches for  $\text{BiFeO}_3$ . Most importantly, we consider another prototypical case of *improper* multiferroic, namely  $\text{HoMnO}_3$ , which has recently attracted much attention.[49, 50] We will show that important differences compared to standard DFT approaches arise when a proper description of correlated electrons, such as that given by HSE, is taken into account.

Our study suggests that HSE functional improves the description compared to standard DFT approaches for multiferroic systems.

The paper is organized as follows. Details of the computational setups are given in

Sect. II. An extended discussion of the structural, electronic, magnetic and ferroelectric properties of BiFeO<sub>3</sub> is reported in Sect. III. Sect. IV is devoted to HoMnO<sub>3</sub> focussing on the paraelectric AFM-A (Sect. IV A) and ferroelectric AFM-E (Sect. IV B) phases. Finally, in Sect. V, we draw our conclusions.

## II. COMPUTATIONAL DETAILS

All the calculations presented in this study are performed by using the latest version of the *Vienna ab initio simulation package* (VASP 5.2).[51] For BiFeO<sub>3</sub>, all the results are obtained using the projector-augmented plane-wave method[52, 53] by explicitly treating 15 valence electrons for Bi ( $5d^{10}6s^26p^3$ ), 14 for Fe ( $3p^63d^64s^2$ ), and 6 for oxygen ( $2s^22p^4$ ). We used a  $6\times 6\times 6$  Monkhorst-Pack  $\mathbf{k}$ -mesh for the Brillouin-zone integration and 400-eV energy cutoff. Tests using a  $8\times 8\times 8$  mesh as well as 600 eV cutoff did not give significant differences in the calculated properties. Brillouin zone integrations are performed with a Gaussian broadening of 0.1 eV during all relaxations. The experimental unit cell for the *R3c* (ferroelectric phase) was used as an input in the full-optimization procedure. For this phase as well as for the paraelectric one (see below), we used the rhombohedral setting. The geometries were relaxed until all force components were less than 0.01 eV/Å and the stress tensor components less than 50 meV/cell. The spin configuration was fixed in order to reproduce the G-type antiferromagnetic state of BiFeO<sub>3</sub> and the spin-orbit coupling was neglected. For the paraelectric phase, we used the non-polar  $R\bar{3}c$  LiNbO<sub>3</sub> phase.[54] We compute the *difference* of electric polarization, *i.e.*  $\Delta P = P^{FE} - P^{PE} = (P_{ion}^{FE} + P_{ele}^{FE}) - (P_{ion}^{PE} + P_{ele}^{PE}) = \Delta P_{ion} + \Delta P_{ele}$ , where *FE*, *PE*, *ion* and *ele* denote ferroelectric, paraelectric, ionic and electronic contribution, respectively. For the paraelectric phase, we used the same lattice constant and rhombohedral angle of the ferroelectric one. Note that, although counterintuitively,  $P_{ele}^{PE}$  may be different from zero, as explained in Ref. 55.  $P_{ion}^{FE,PE}$  is calculated by summing the position of each ion in the unit cell times the number of its valence electrons. The electronic contribution is obtained by using the Berry phase formalism, within the “modern” theory of polarization.[56–58]

Concerning the HSE calculations, due to the high computational load,[97] we always used the 400 eV and  $6\times 6\times 6$   $\mathbf{k}$ -point mesh. The Fock exchange was sampled using the twofold reduced  $\mathbf{k}$ -point grid (using the full grid, gives however negligible changes in the computed

properties). Finally, we performed  $G_0W_0$  calculations[59–64] on top of the HSE electronic and ionic structure, which usually represent a good starting point for a perturbative quasi-particle excitation energies.[60] We also included vertex correction in  $W$  via an effective nonlocal exchange correlation kernel.[63]

For orthorhombic  $\text{HoMnO}_3$ , the  $Pnma$  symmetry is chosen with the  $b$  basis vector as the longest one. The paraelectric phase was simulated using 20-atoms cell in the AFM-A spin configuration showing ferromagnetic (FM) (AFM) intraplanar (interplanar) coupling; for the ferroelectric one we used a 40-atoms cell (doubling the previous cell along the  $a$  axis) in the AFM-E spin configuration (*i.e.* in-plane FM zigzag chains anti-ferromagnetically coupled to the neighboring chains with the interplanar coupling also AFM). The energy cutoff was set to 300 eV and the Brillouin zone mesh was fixed to  $4 \times 2 \times 4$  and  $2 \times 2 \times 4$  grid for the AFM-A and AFM-E phase respectively. Ho  $4f$  electrons were assumed as frozen in the core. The experimental lattice constants were used for all the calculations but the internal positions were relaxed. For the HSE calculations, the Fock operator was evaluated on the down-folded  $\mathbf{k}$ -point mesh. In order to assess the relative stability of the two magnetic phases, we used the same simulation cell containing 40 atoms for both phases, increasing the cutoff to 400 eV and using a  $4 \times 2 \times 4$   $\mathbf{k}$ -point grid.

### III. $\text{BIFeO}_3$ : RESULTS AND DISCUSSIONS

#### A. Structural properties

The ferroelectric structure is represented by a distorted double perovskite structure with  $R3c$  symmetry (N. 161, point group  $C_{3v}$ ) as reported by Kubel and Schmid.[65] The paraelectric phase has  $R\bar{3}c$  symmetry (N. 167, point group  $D_{3d}$ ). Both phases are shown in Fig.1. In Table I we report relevant properties such as the structural parameters, the Fe magnetic moment and the energy gap calculated using the PBE and HSE functionals. We also report the values using the B1-WC functional taken from Ref.[46]

First of all, HSE reduces the lattice parameter  $a_{rh}$  with respect to PBE, giving a much better agreement with the experimental value: the error decreases from  $\sim 1$  %(PBE) to  $\sim 0.3$  %(HSE). As a consequence, the unit cell volume  $V$  also shrinks, getting closer to the experimental value. The rhombohedral angle,  $\alpha_{rh}$ , is almost insensitive to the applied

functional. Thus, the inclusion of Fock exchange makes the structure more compact, *i.e.* the lattice constant decreases. Note that the B1-WC functional gives too small lattice constant and too small equilibrium volume as compared to HSE, worsening the comparison with the experiments. There is a very good agreement between the relaxed coordinates of the Wyckoff positions and the experimental ones using HSE, while the PBE as well as the B1-WC functional give slightly worse results ( the only exception being the  $x$  component of the oxygen atoms in the  $6b$  site symmetry). In the experimental structure, the  $\text{BiO}_6$  cage is strongly distorted with three coplanar nearest neighbors (NNs) lying above Bi along  $[111]$  at  $2.270 \text{ \AA}$  ( $d_{\text{Bi-O}}^s$ ,  $s$  refers to short) and three NNs sitting below at  $2.509 \text{ \AA}$  ( $d_{\text{Bi-O}}^l$ ,  $l$  refers to long). From Table I, we see that the theoretical NNs distances compare well with experiments, with errors from  $\sim 1 \%$  to  $\sim 4 \%$  (PBE), from  $\sim 3 \%$  to  $\sim 5 \%$  (B1-WC) and  $\sim 2 \%$  (HSE). The  $\text{O}-\widehat{Fe}-\text{O}$  bond angle would be  $180^\circ$  in the ideal cubic perovskite. In this system, it buckles to an experimental value of  $165.03^\circ$ . The HSE value ( $164.56^\circ$ ) is close to PBE, and in both cases, they are slightly underestimated with respect to experiment. The B1-WC angle, on the other hand, is clearly underestimated. Overall, the predicted HSE values clearly are in much better agreement with experiments than those calculated using the PBE or B1-WC functional.

## B. Electronic and magnetic properties

Let us consider now the magnetic and electronic properties. As shown in Table I, the calculated local moments are generally very similar for all the functionals, and close to the experimental value. In particular, the HSE local moment is slightly larger than PBE, suggesting a more localized picture of the spin-polarized electrons. The calculated PBE (HSE) electronic energy gap is 1.0 (3.4) eV. The expected band-gap opening using hybrid functionals can be understood as follows: the exact exchange acts on occupied states only, correcting them for the self-interaction, thus shifting downwards the occupied valence bands. In turn, this has a clear interpretation: within the Hartree-Fock approximation for the ground state of an  $N$  electron system, the potential felt by each of the  $N$  electrons in the ground state is that due to  $N-1$  other electrons, *i.e.* they feel a more attractive ionic potential. On the other hand, for unoccupied states, the potential is that due to the  $N$  occupied orbitals, so these orbitals effectively experience a potential from one more electron, the latter screens

the ionic potential which in turn becomes less attractive. Therefore, the unoccupied states are shifted upwards, opening the gap.

As for the experimental energy gap for BiFeO<sub>3</sub>, the situation is not clear. There have been several measurements of the band gap using UV-visible absorption spectroscopy and ellipsometry on polycrystalline BFO films, epitaxial BFO films grown by pulsed-laser deposition, nanowires, nanotubes, and bulk single crystals. Reported band-gap values vary from 2.5 to 2.8 eV.[66–71] An estimate gives  $\sim 2.5$  eV from the optical absorption spectra by Kanai *et al.*[70] and Gao *et al.* [71]. From the theoretical side, there is a spread of values: a small gap of 0.30-0.77 eV using LSDA,[55] or from 0.3 to 1.9 eV using “LDA+U”, depending on the value of U[55]; 0.8-1.0 eV using PBE (WC) GGA functional;[45] 3.0-3.6 eV using B1-WC and B3LYP hybrid functionals.[45] Thus, a parameter-free theoretical reference value is clearly needed. The most accurate (but expensive) method is the GW approximation.[59] Here, we provide for the first time, the value of the BFO energy gap based on the GW method.

First of all, at the PBE level, we estimate an energy gap of 1.0 eV. When introducing the exact exchange (HSE), the gap opens up to  $E_g=3.4$  eV. Upon inclusion of many-body effects ( $G_0W_0$ ), it opens even more ( $E_g=3.8$  eV). Finally, when including vertex corrections, we find that the gap reduces to 3.3 eV. Remarkably, vertex corrections almost confirm the HSE band gap. This is perfectly in line with recent works[40] where it is argued that HSE band gaps represent a very accurate estimate due to partial inclusion of the derivative discontinuity of the exchange-correlation functional.[8] Clearly, effects beyond bare DFT are important in this compound. Our results show that hybrid-functional calculations give already a very good estimate at a lower computational cost compared to GW. In this respect, we mention the very recent experimental study based on resonant soft x-ray emission spectroscopy[72] where the band gap corresponding to the energy separation between the top of the O  $2p$  valence band and the bottom of the Fe  $d$  conduction band is 1.3 eV. The discrepancy between theory and experiment may be due to the presence of defects in the experimental sample as well as to the resolution involved in photoemission spectra. We hope to stimulate further experimental work to test our first-principles prediction of the energy gap of this important multiferroic material.

In Fig. 2 we show the Density of States (DOS) for the optimized atomic structure. Let’s focus on the PBE DOS. The lowest states at  $\sim -10$  eV are Bi  $s$  hybridized with O  $p$  states

(blue curve). Above  $-6$  eV there are hybridized O  $p$  and Fe  $d$  states. The Fe  $d$  states extend in the conduction band as well; the Bi  $p$  states can be found above 4 eV. As for the HSE DOS, we see that the conduction bands are shifted upwards, opening the valence-conduction gap. There is a change in the spectral distribution above  $-8$  eV: a valley appears around  $-6$  eV and the lower shoulder of the peak increases its spectral weight. It is easy to trace back the above changes to modifications of the majority Fe  $d$  states, as shown in the panel beneath: while in PBE the band states in the vicinity of the top of the valence band have predominantly  $d$  character, in HSE the spectral weight of the Fe  $d$  states is concentrated far away from the top of the valence band. This can be interpreted as a change from a more itinerant picture to a more localized description of the Fe  $d$  states going from PBE to HSE. In Fig. 2, we also include the spectral distribution of the Fe  $d$  states derived from a recent experimental work[72] (see dotted lines): the position of the main HSE Fe  $d$  peak almost perfectly matches the experimental PDOS, although the bandwidth of the calculated DOS is different because of energy resolution, etc. Indeed, if we include the Fe  $d$  DOS calculated using  $G_0W_0+$  vertex corrections, the agreement between the theoretical and experimental peak position becomes excellent. Note that the HSE and  $G_0W_0+$ Vertex peak position are very close to each other, confirming the accurate HSE description of the  $\text{BiFeO}_3$  electronic structure. In passing we note that while DFT+ $U$  gives a better estimate of the Fe  $d$  peak position,[55] the energy gap is still underestimated with respect our GW calculation.

We previously mentioned that HSE may change the ionic/covalent character in this compound. To support this, in Fig. 3 we show the difference between the PBE and HSE charge density,  $\Delta\rho = \rho^{PBE} - \rho^{HSE}$  calculated at fixed geometry. In a purely ionic description, all the valence electrons would be located on the oxygens, acting as “electron sinks”, and the cations would donate their nominal valence charge. The more the electrons populate the anions, or conversely, the more the electrons depopulate the cations, the more the picture shows an ionic character. Fig. 3 confirms the trend discussed before: upon adding a fraction of exact exchange to the PBE functional, the electronic charge at the cations decreases, *i.e.*  $\Delta\rho$  is positive (grey areas in Fig. 3), while the electronic charge at the anions increases *i.e.*  $\Delta\rho$  is negative (yellow areas in Fig. 3). Thus, the introduction of exact-exchange generates a flux of charge from the cations towards the anions, clearly shown in Fig. 3, increasing the ionicity of the compound.

In order to discuss more quantitatively these effects, we perform a Bader analysis of

the electronic charge.[73–75] The atom in molecules (AIM) theory is a well established analysis tool for studying the topology of the electron density and suitable for discussing the ionic/covalent character of a compound. The charge ( $Q_B$ ) enclosed within the Bader ( $V_B$ ) volume is a good approximation to the total electronic charge of an atom. In Table II we report  $Q_B$  and  $V_B$  calculated for Bi, Fe, and O at a fixed geometric structure, *i.e.* HSE geometry. This is needed in order to avoid different volumes for the normalization of the charge in the unit cell and for highlighting the electronic structure modifications due to the exact exchange. Furthermore, we consider only the valence charge for our analysis (although one should formally include also the core charge, we do not expect variations as far as the trends are concerned). Let us first consider the cations: the Bader charge and volume are larger in PBE than in HSE. For the anions, the opposite holds true. This is not unexpected and in agreement with intuition: upon introducing Fock exchange, the system evolves towards a more ionic picture, through a flux of charge from cations towards anions, which reduces (increases) the “size” of the cations (anions) when going from the PBE to the HSE solution. Finally, we note that a different degree of ionicity modifies the calculated equilibrium lattice parameter: in a partially covalent material, such as BiFeO<sub>3</sub>,[76] the increased ionicity changes the different net charges generating a higher Madelung field, which is an important contribution to the bonding in the solid, and contracts the equilibrium structure.[77, 78]

### C. Ferroelectric properties

Let’s finally focus on the electric polarization. In Table IV, we report the ionic and electronic contributions to the difference of ferroelectric polarization between the polar ( $R3c$ ) and non-polar ( $R\bar{3}c$ ) both in PBE and HSE. In order to disentangle the purely electronic effects from the ionic ones upon introduction of Fock exchange, we report also the PBE(HSE) electronic contribution calculated at fixed HSE(PBE) geometry.

As a general comment, we note that a large polarization of  $\sim 100 \mu C/cm^2$  along (111) for bulk BFO has been reported experimentally by new measurements on high-quality single crystals.[79] in good agreement with our calculated values. In what follows, we will mainly focus on the differences between PBE and HSE calculations. Note that the unit cell volume is different for PBE and HSE, as shown in Table I.

First, we note that the polarization calculated according to the point charge model ( $P_{pcm}$ ) is closer to  $P_{tot}$  at the HSE than at the PBE level. This confirms that the HSE description of BFO points towards an ionic picture, *i.e.* by decreasing the covalency effects. The calculated total polarization  $P_{tot}$  is  $\sim 105 \mu C/cm^2$  using PBE and  $\sim 110 \mu C/cm^2$  using HSE, *i.e.* HSE predicts an increase of *total* electric polarization. The occurrence of ferroelectricity in  $BiFeO_3$  is usually discussed in terms of “polarizable lone pair” carried by the Bismuth atom. This has a physical interpretation in terms of cross gap hybridization between occupied O  $2p$  states and unoccupied Bi  $6p$  states.[76, 80–83]. Intuitively, the larger the energy gap, the lower the polarization should be. Accordingly, one might expect HSE to reduce the polarization compared to PBE because of the larger energy gap. We will show below that this is not in contradiction with the results of Table I. In fact, let’s consider  $P_{tot}$  calculated at the *same* atomic structure (for example at the PBE relaxed structure of the paraelectric and ferroelectric phases) but using both PBE and HSE. We denote the former as  $P_{tot}^{PBE}$ , the latter as  $P_{tot}^{HSE(PBE)}$ . Note that the ionic contributions is of course the same for both cases. From Table I, we have  $P_{tot}^{PBE}=105.6 \mu C/cm^2$  and  $P_{tot}^{HSE(PBE)}=103.2 \mu C/cm^2$ , *i.e.* a decrease of total polarization is found in going from PBE to HSE for the same ionic structure. A similar behavior is found in opposite conditions: for the HSE ionic structure,  $P_{tot}^{HSE}=110.3 \mu C/cm^2$  and  $P_{tot}^{PBE(HSE)}=112.6 \mu C/cm^2$ . Thus, keeping the same volume and including Fock exchange, the polarization reduces as expected. On the other hand, when we evaluate the *total* polarization at the appropriate equilibrium and relaxed structures using PBE and HSE, the ionic contribution also varies and one loses a direct connection between the increase of the energy gap and the decrease of total polarization. In our case, the total polarization, when evaluated at the appropriate equilibrium volume for each functional, increases from PBE to HSE. This clearly points out a strong volume-dependence of the polarization, therefore calling for a correct estimate of the volume (as provided by HSE).

## IV. $\text{HoMnO}_3$ : RESULTS AND DISCUSSIONS

### A. Paraelectric AFM-A phase

#### 1. Structural properties

An extended review of the main properties of orthorhombic  $\text{HoMnO}_3$  within a standard PBE approach can be found in Ref. [84] where it is also shown that the inclusion of the  $U$  correction worsens the structural properties. Therefore, in this paper, we will focus on the comparison between the predictions of HSE with respect to PBE results. In Fig. 4 we show the perspective view of  $\text{HoMnO}_3$  and the paraelectric (AFM-A) and ferroelectric (AFM-E) spin configurations in the  $c - a$  plane.

In Table III we report the optimized structural parameters in the AFM-A magnetic configuration, calculated using PBE and HSE. The in-plane short ( $s$ ) and long ( $l$ ) Mn-oxygen bond-lengths get closer to experimental values using HSE; on the other hand, the out-of-plane length is slightly overestimated with respect to the PBE and the experimental value. In order to quantify structural distortions, the Jahn-Teller (JT) distortion vector  $\mathbf{Q} = [Q_1, Q_2] = [\sqrt{l-s}, \sqrt{\frac{2}{3}}(2m-l-s)]$  is often introduced. From Table III, it is thus clear that the HSE functional improves the JT distortion upon the PBE description: the magnitude of  $\mathbf{Q}$  is  $Q=0.55 \text{ \AA}$  and  $0.61 \text{ \AA}$  using PBE and HSE, respectively, whereas the experimental value is  $0.59 \text{ \AA}$ . As far as the structural angles are concerned, we first notice that the  $\text{GdFeO}_3$ -like tilting ( $\alpha$ ) in the  $\text{Mn-O}_6$  octahedron is slightly overestimated using the hybrid functional: the deviation from the experimental angle is 3.7 (PBE) and 5.0 % (HSE) with the Mn-O-Mn in-plane angles calculated using HSE slightly reduced with respect to PBE. We note, however, that the experimental uncertainty on the angles may be up to  $\sim 1^\circ$ , [85] due to synthesis problems of ortho- $\text{HoMnO}_3$ . [50, 85] The octahedral tilting is related to the ionic size of the rare-earth ion:[86, 87] the tilting increases when the radius of the rare-earth atom decreases (for example, from La to Lu in the manganites series).[84] In this respect, the tendency towards a larger octahedral tilting, upon inclusion of exact-exchange-functional, goes hand in hand with the reduced ionic size of Ho ion when going from PBE to HSE. As in the previous case, we performed a Bader analysis of the valence charge distribution. Results are shown in Table II: as expected, the "size" of the Ho ion is reduced within HSE. According to our previous discussion, the ionic/covalent character

of the charge density is modified by HSE in favor of a more ionic picture. This will have important consequences for the electronic polarization, as shown below.

## 2. Electronic properties

In Fig. 5 we show the band structure for the AFM-A phase as calculated using standard PBE (left panel) as well as HSE (right panel) along the main symmetry lines. The PBE band structure shows a small gap equal to  $\sim 0.2$  eV. The bands below  $\sim -2$  eV are mainly oxygen  $p$  states and those 2-3 eV below (above) the Fermi level are mainly spin-up (spin-down) Mn  $d$  states. There is also a considerable weight of the Mn  $d$  states in the oxygen bands near the top of the valence band.[98]

The group of bands between  $-1$  and  $-2$  eV are mainly  $d_{xy}, d_{yz}$  with some small weight of  $d_{z^2}$ . The two bands just below the Fermi energy are mainly  $d_{x^2-y^2}$ -like with some  $d_{xz}$  weight; at  $Y, S, Z$  they become degenerate. Higher in energy, between 0 and 1 eV, there are two more bands showing a similar behavior, *i.e.* degenerate at  $Y, S, Z$ , almost degenerate along  $Z-R$  and with a similar overall band dispersion. Even higher in energy, they are the Mn minority states. From Fig. 5, we can extract the JT splitting ( $\Delta_{JT}$  of the “ $e_g$ ” states), the CF splitting ( $\Delta_{CF}$  between “ $e_g$ ” and “ $t_{2g}$ ”), and the exchange splitting ( $\Delta_{EX}$  between majority and minority spin states, evaluated at the  $S$  point, for simplicity). We thus have  $\Delta_{JT}=1.05$ ,  $\Delta_{CF}=2.34$ , and  $\Delta_{EX}=2.75$  eV. The comparison between the PBE and HSE band structure highlights some differences. First we note that the oxygen bands are slightly shifted to lower binding energy together with the Mn  $d_{xy}, d_{yz}$  bands. On the other hand, the average position of occupied Mn  $d_{xz}, d_{x^2-y^2}$  bands remain almost unchanged, but the band-width increases. The latter effect is mainly shown by the lowest of the two bands, *i.e.* the  $d_{xy}$ -like band. As well known,[88] Hartree-Fock hamiltonians naturally leads to larger band-width and down-shift of electronic states, even for simple homogeneous systems. Thus, the larger band-widths obtained by HSE can not be simply connected to a stronger hybridization, because it is an intrinsic feature of Fock exchange for every electronic state. Indeed, we will show below that the  $d-p$  hybridization is expected to decrease using HSE.

$\Delta_{JT}$  is evaluated as 3.4 eV, larger than in the PBE case, suggesting a stronger local distortion related to the Jahn-Teller instability. The increase of the JT splitting is linked to the increase of the energy gap as well, which is now  $\sim 2.7$  eV. The exchange splitting,

$\Delta_{EX}=4.6$  eV, is also larger along with an increased local Mn moments with respect to PBE. Note, that the enhancement of Jahn-Teller distortion by HSE is not unexpected. In fact, it was previously suggested that the HSE functional is able to reveal the Jahn-Teller effect for  $\text{Mn}^{+4}$  through a *symmetry broken solution* giving rise to an orbitally ordered state and consequent Jahn-Teller distortion.[37] The larger  $\Delta_{JT}$  is mainly driven by a purely electronic effect due to the inclusion of Fock-exchange. Infact, by calculating the PBE self-consistent charge density on top of the HSE ionic structure,  $\Delta_{JT}$  becomes  $\sim 1.2$  eV, *i.e.* nearly equal to the previous PBE case. Thus, we expect HSE to cause a rearrangement of the charge density that will *reduce* the electronic contribution to the electronic polarization when considering the polar phase. This can be understood as follows. The increase of the Jahn-Teller splitting goes hand in hand with the increase of the energy gap: the larger the gap, the smaller the dielectric constant is, *i.e.* the smaller the screening is. Now, let us consider the fixed ionic configuration of the paraelectric phase: the charge in the non-centrosymmetric *spin arrangement* can be thought as a “small” perturbation of the centrosymmetric one upon the application of the “internal” electric field. The electronic charge will respond to such a field, and each electronic state will change assuming a polarized configuration. If the gap is large, the “electric field” will hardly mix the electronic states in the valence band with the electronic states in the conduction band, since in second order perturbation theory approach the denominator will be of order of the band gap energy, so that the electrons don’t polarize much, *i.e.* the charge distribution becomes more “rigid”. In conclusion, we expect the electronic contribution to the electric polarization to decrease upon introduction of Fock exchange. This will be confirmed by our calculations. Note that the above reasoning is not appropriate for BFO where the polarization is mainly due to ionic displacements.

## B. AFM-E phase

### 1. Structural properties

Let us focus on the AFM-E phase, where the resulting symmetry is lowered by the spin configuration with respect to the AFM-A spin arrangements by removing the inversion symmetry. In Fig. 6, we show the relevant structural internal parameters, for the relaxed PBE and HSE structure, by considering the Mn-O-Mn-O-Mn chain (compare Fig. 6 and Fig.

4). The Mn-O *short* bond-lengths do not show significant differences between the parallel and antiparallel spin configuration in PBE as well in HSE. On the other hand, the long Mn-O bond lengths are mostly affected: their difference,  $l^p - l^{ap}$  in PBE is about 0.07 Å and decreases to  $\sim 0.02$  Å upon introduction of exact exchange. At the same time, the angle changes:  $\alpha^p$  decreases while  $\alpha^{ap}$  remains almost equal to the PBE value. The results can be interpreted as follows: bare PBE is expected to overestimate hybridization effects between oxygen  $p$ -states and Mn  $d$ -states, therefore inducing a stronger rearrangement of ionic positions consistent with a “softer” structure when moving from, say a centrosymmetric A-type to a ferroelectric E-type phase. Viceversa, upon introduction of correlation effects, the reduced hybridization is expected to lead to a more “rigid” ionic arrangement. Indeed, this is evident when comparing the difference between  $\alpha^p - \alpha^{ap}$ , which drastically reduces upon introduction of HSE with respect to PBE. We recall that, ultimately, it is this difference that gives rise to the ionic polarization, as clearly shown in Fig. 2 b) of Ref.[49]. We can therefore anticipate that a reduction of the polarization will occur upon introduction of HSE, as discussed in detail below. What is worthwhile noting is that the Mn-Mn distances in PBE dramatically depends on their having parallel ( $d_{Mn-Mn}^p = 3.98$  Å) or antiparallel spins ( $d_{Mn-Mn}^{ap} = 3.87$  Å), so that  $d_{Mn-Mn}^p - d_{Mn-Mn}^{ap} = 0.11$  Å. However, this dependence is smoothed upon introduction of HSE, so that the difference in Mn-Mn distance strongly reduces to  $d_{Mn-Mn}^p - d_{Mn-Mn}^{ap} = 0.03$  Å. In general, the marked (weak) dependence of the structural properties within PBE (HSE) is consistent with a strong (small) efficiency of the double-exchange mechanism, which ultimately relies on the  $p-d$  hybridization and hopping integral.

## 2. *Electronic and magnetic properties*

The band-structure of the AFM-E is quite similar to the A-type and is therefore not shown. However, there are some small differences which we comment on. As expected, the increase of the number of the AFM bonds of each Mn with its four neighbors associated with the change of the magnetic state going from AFM-A to AFM-E type results in a narrowing of all bands. This is further enhanced by HSE due to the reduced hopping upon introduction of exact exchange, as expected. Furthermore, the increase of the band gap is facilitated by the interplay of the crystal distortion, which is generally enhanced by HSE, with the AFM

arrangement of spins. As expected, the energy gap is the largest in the AFM-E-HSE band structure, being now  $\sim 3$  eV. The  $\Delta_{JT}$  evaluated at  $S$  point, is also the largest in this case, being  $\sim 3.7$  eV. Before turning our attention to the electronic polarization, we discuss the magnetic properties. First of all, we found that the AFM-E is more stable than the AFM-A by  $\sim 4$  meV/cell in the HSE formalism. Note that this value has been obtained using the same simulation cell for both phases, therefore reducing the influence of numerical errors. Although the relative stability is still comparable with the numerical accuracy, it is indeed consistent with experiments.[50, 85] In AFM-E-PBE, the Mn moment is  $3.4 \mu_B$  which induces a small spin-polarization on the oxygen equal to  $\pm 0.04 \mu_B$ . In AFM-E-HSE, the Mn moment slightly increases to  $3.7 \mu_B$  and the oxygen moment slightly decreases to  $\pm 0.01 \mu_B$ : the increased localization of the Mn  $d$  states correlates with the increased Manganese spin moment and goes hand by hand with the decreased  $p$ - $d$  hybridization and a decreased induced spin moment on oxygens.

### 3. Ferroelectric properties

Finally, we calculated the ferroelectric polarization by considering the AFM-A as the reference paraelectric structure. The results show that the polarization (both the electronic and ionic terms) strongly reduces upon introduction of HSE. However, it is remarkable that the total  $P$  is still of the order of  $2 \mu C/cm^2$ : this confirms  $HoMnO_3$  as the magnetically-induced ferroelectric having the highest polarization predicted so far. Our estimate is in very good agreement with model Hamiltonian calculations.[89] The comparison between theory and experiments as far as the electric polarization is concerned is still a matter of debate. Whereas earlier studies predicted negligible values for polycrystalline  $HoMnO_3$  samples,[90] more recent studies for  $TmMnO_3$  in the E-type (where the exchange-striction mechanism is exactly the same as in  $HoMnO_3$ ) point to a polarization which could exceed  $1 \mu C/cm^2$ ,[91] in excellent agreement with our predicted HSE value.

The reasons why we expect a reduction upon introduction of HSE have been already discussed in previous paragraphs and can be traced back to the reduced  $p-d$  hybridization. As in the case of BFO, we disentangle the structural and electronic effects, by using the HSE (PBE) geometry with the PBE (HSE) functional (cfr. Table IV). What we infer from these “ad-hoc”-built systems is that the use of HSE dramatically reduces the electronic con-

tribution (cfr  $P_{ele}$  in PBE and HSE(PBE)), *i.e.* reduced by  $\sim 2.5 \mu C/cm^2$ . Less important, though still appreciable, seem to be the ionic displacements: their dipole moment is reduced by  $\sim 1.5 \mu C/cm^2$  when comparing  $P_{tot}$  in HSE and HSE(PBE). This is consistent with what shown approximately by  $P_{pcm}$ .

## V. CONCLUSIONS

In this work, we have revised the two workhorse materials of the exponentially growing field of multiferroics, namely BiFeO<sub>3</sub> for proper MFs and HoMnO<sub>3</sub> for improper MFs by using the screened hybrid functional (HSE).

From our study, several important points emerge. For BFO: i) the structural, electronic and magnetic properties well agree with experiments; ii) the ferroelectric polarization agrees with reported values in the literature; iii) even if PBE allows the description of ferroelectric properties by opening an energy gap, it is by no means satisfactory in correctly describing all the properties on the same footing. On the other hand, HSE improves the PBE and LDA+ $U$  description; this is clearly shown by benchmark calculations using the most advanced and accurate state-of-the art GW+vertex corrections (which basically confirm the HSE results); iv) the previous comment, and very recent studies[40] suggests that optical properties, so far not investigated at all by ab-initio calculations for BFO, can be properly addressed within HSE. v) finally, we note that the electronic polarization *increases* upon introduction of exact exchange. For HMO, we note that: i) the HSE results are in good agreement with experiments when available; ii) the Jahn-Teller effect is correctly described in agreement with experiment; iii) despite a reduction of the polarization value with respect to PBE, HoMnO<sub>3</sub> still shows the highest  $P$  predicted among magnetically-induced ferroelectrics.

We have shown that introduction of "correlation" effects may both enhance the polarization or reduce it: the former effect will most likely occur for proper MFs, and the latter for improper MFs, *e.g.* magnetically driven. Note that an increase of HSE polarization with respect to LDA, for example, is also found by Wahl *et al.*[43] for BaTiO<sub>3</sub>, a standard ferroelectric compound. Also for BiFeO<sub>3</sub>, an increase of polarization using DFT+ $U$  has been noticed.[55, 76, 92] The increase of ferroelectric polarization when including a fraction of exact exchange and using the theoretical equilibrium volume has been reported also for simple ferroelectric compound such as KNbO<sub>3</sub>. [77]

One final comment is in order: although the HSE results certainly point towards a truly realistic description, it is still possible that, to some extent, the good performances of HSE may be material-dependent, *i.e.* the universal 1/4 fraction of the exact exchange may be not appropriate for some specific material. What is certainly true is that the predictive capability of HSE, combined with its nowadays affordable computational costs, make the functional an attractive choice for the study of a wide range of materials, from well-behaved insulators to doped semiconductors exhibiting magnetic ordering, multifunctional complex oxides of interest for many industrial applications therefore representing a very good starting point for materials design.

### **Acknowledgments**

The research leading to these results has received funding from the European Research Council under the European Community, 7th Framework Programme - FP7 (2007-2013)/ERC Grant Agreement n. 203523. A.S. would like to thank G. Kresse for kind assistance for the GW calculations and M. Marsman for useful discussions. Furthermore, A.S. thanks L. Kronik (Weizmann Institute) for helpful comments. The authors acknowledge kind hospitality at the S<sup>3</sup> CNR-INFN National Center in Modena after the catastrophic earthquake of April 6<sup>th</sup> 2009 in L'Aquila. The computational support by Caspur Supercomputing Center in Roma and technical assistance by Dr. L. Ferraro is gratefully acknowledged. Figures have been done by using the VESTA package.[93]

- 
- [1] D. I. Khomskii, *Physics*, 2009, **2**, 20.
- [2] T. Kimura, T. Goto, H. Shintani, K. Ishizaka, T. Arima and Y. Tokura, *Nature (London)*, 2003, **426**, 55.
- [3] N. Hur, S. Park, P. A. Sharma, J. S. Ahn, S. Guha and S.-W. Cheong, *Nature (London)*, 2004, **429**, 392.
- [4] S.-W. Cheong and M. Mostovoy, *Nat. Mat.*, 2007, **6**, 13.
- [5] J. Wang, J. Neaton, H. Zheng, V. Nagarajan, S. B. Ogale, B. Liu, D. Viehland, V. Vaithyanathan, D. G. Schlom, U. V. Waghmare, et al., *Science*, 2005, **307**, 1203b.
- [6] M. Fiebig, *J. Phys. D: Appl. Phys.*, 2005, **38**, R123.
- [7] N. A. Spaldin and M. Fiebig, *Science*, 2005, **309**, 391.
- [8] S. Kümmel and L. Kronik, *Rev. Mod. Phys.*, 2008, **80**, 3.
- [9] G. B. Bachelet and N. E. Christensen, *Phys. Rev. B*, 1985, **31**, 879.
- [10] A. Filippetti and N. A. Hill, *Phys. Rev. B*, 2002, **65**, 195120.
- [11] W. G. Aulbur, L. Jónsson and J. W. Wilkins, *Solid State Physics*, 1999, **54**, 1.
- [12] F. Aryasetiawan and O. Gunnarsson, *Rep. Prog. Phys.*, 1998, **61**, 237.
- [13] V. I. Anisimov, F. Aryasetiawan and A. I. Lichtenstein, *J. Phys.: Condens. Matter*, 1997, **9**, 767.
- [14] V. I. Anisimov, J. Zaanen and O. K. Andersen, *Phys. Rev. B*, 1991, **44**, 943.
- [15] I. V. Solovyev, P. H. Dederichs and V. I. Anisimov, *Phys. Rev. B*, 1994, **50**, 16861.
- [16] J. P. Perdew and A. Zunger, *Phys. Rev. B*, 1981, **23**, 5048.
- [17] A. Filippetti and N. A. Spaldin, *Phys. Rev. B*, 2003, **67**, 125109.
- [18] A. Droghetti, C. D. Pemmaraju and S. Sanvito, *Phys. Rev. B*, 2008, **78**, 140404(R).
- [19] A. Rohrbach, J. Hafner and G. Kresse, *Phys. Rev. B*, 2004, **69**, 075413.
- [20] I. A. Kornev, S. Lisenkov, R. Haumont, B. Dkhil and L. Bellaiche, *Phys. Rev. Lett.*, 2007, **99**, 227602.
- [21] A. Svane and O. Gunnarsson, *Phys. Rev. Lett.*, 1990, **65**, 1148.
- [22] C. D. Pemmaraju, T. Archer, D. Sánchez-Portal and S. Sanvito, *Phys. Rev. B*, 2007, **75**, 045101.
- [23] M. Stengel and N. A. Spaldin, *Phys. Rev. B*, 2008, **77**, 155106.

- [24] P. J. Stephens, F. J. Devlin, C. Chabalowski and M. J. Frisch, *J. Phys. Chem.*, 1994, **98**, 11623.
- [25] C. Adamo and V. Barone, *J. Chem. Phys.*, 1999, **110**, 6158.
- [26] M. Ernzerhof and G. E. Scuseria, *J. Chem. Phys.*, 1999, **110**, 5029.
- [27] A. V. Krukau, O. A. Vydrov, A. F. Izmaylov and G. E. Scuseria, *J. Chem. Phys.*, 2006, **125**, 224106.
- [28] J. Muscat, A. Wander and N. M. Harrison, *Chem. Phys. Lett.*, 2001, **342**, 397.
- [29] J. Heyd, J. E. Peralta, G. E. Scuseria and R. L. Martin, *J. Chem. Phys.*, 2005, **123**, 174101.
- [30] J. Paier, M. Marsman, K. Hummer, G. Kresse, I. C. Gerber and J. A. Ángyán, *J. Chem. Phys.*, 2006, **124**, 154709.
- [31] P. J. Hay, R. L. Martin, J. Uddin and G. E. Scuseria, *J. Chem. Phys.*, 2006, **125**, 034712.
- [32] I. D. Prodan, G. E. Scuseria and R. L. Martin, *Phys. Rev. B*, 2006, **73**, 045104.
- [33] I. D. Prodan, G. E. Scuseria and R. L. Martin, *Phys. Rev. B*, 2007, **76**, 033101.
- [34] M. Marsman, J. Paier, A. Stroppa and G. Kresse, *J. Phys.: Condens. Matter.*, 2008, **20**, 064201.
- [35] A. Stroppa, K. Termentzidis, J. Paier, G. Kresse and J. Hafner, *Phys. Rev. B*, 2007, **76**, 195440.
- [36] A. Stroppa and G. Kresse, *New J. Phys.*, 2008, **10**, 063020.
- [37] A. Stroppa and G. Kresse, *Phys. Rev. B (R)*, 2009, **79**, 201201(R).
- [38] A. D. Becke, *J. Chem. Phys.*, 1993, **98**, 1372.
- [39] M. Ernzerhof, K. Burke and J. P. Perdew, *J. Chem. Phys.*, 1996, **105**, 9982.
- [40] B. J. Janesko, T. M. Henderson and G. Scuseria, *Phys. Chem. Chem. Phys.*, 2009, **11**, 443.
- [41] J. Heyd, G. E. Scuseria and M. Ernzerhof, *J. Chem. Phys.*, 2003, **118**, 8207.
- [42] J. Heyd, G. E. Scuseria and M. Ernzerhof, *J. Chem. Phys.*, 2006, **124**, 219906.
- [43] R. Wahl, D. Vogtenhuber and G. Kresse, *Phys. Rev. B*, 2008, **78**, 104116.
- [44] J. P. Perdew, K. Burke and M. Ernzerhof, *Phys. Rev. Lett.*, 1996, **77**, 3865.
- [45] D. I. Bilc, R. Orlando, R. Shaltaf, G.-M. Rignanese, J. Íñiguez and P. Ghosez, *Phys. Rev. B*, 2008, **77**, 165107.
- [46] M. Goffinet, P. Hermet, D. I. Bilc and P. Ghosez, *Phys. Rev. B*, 2009, **79**, 014403.
- [47] Z. Wu and R. E. Cohen, *Phys. Rev. B*, 2006, **73**, 235116.
- [48] E. Heifets, E. Kotomin and V. A. Trepakov, *J. Phys.: Condens. Matter*, 2006, **18**, 4845.

- [49] S. Picozzi, K. Yamauchi, B. Sanyal, I. A. Sergienko and E. Dagotto, *Phys. Rev. Lett.*, 2007, **99**, 227201.
- [50] A. Munoz, M. Casáis, J. A. Alonso, M. J. Martínez-Lope, J. L. Martínez and M. Fernández-Díaz, *Inorg. Chem.*, 2001, **40**, 1020.
- [51] G. Kresse and J. Furthmüller, *Phys. Rev. B*, 1996, **54**, 11169.
- [52] P. E. Blöchl, *Phys. Rev. B*, 1994, **50**, 17953.
- [53] G. Kresse and D. Joubert, *Phys. Rev. B*, 1999, **59**, 1758.
- [54] H. Boysen and F. Altorfer, *Acta Cryst. B*, 1994, **50**, 405.
- [55] J. B. Neaton, C. Ederer, U. V. Waghmare, N. A. Spaldin and K. M. Rabe, *Phys. Rev. B*, 2005, **71**, 014113.
- [56] R. D. King-Smith and D. Vanderbilt, *Phys. Rev. B*, 1993, **47**, 1651.
- [57] D. Vanderbilt and R. D. King-Smith, *Phys. Rev. B*, 1993, **48**, 4442.
- [58] R. Resta, *Rev. Mod. Phys.*, 1994, **66**, 899.
- [59] M. S. Hybertsen and S. G. Louie, *Phys. Rev. B*, 1986, **34**, 5390.
- [60] F. Fuchs, J. Furthmüller, F. Bechstedt, M. Shishkin and G. Kresse, *Phys. Rev. B*, 2007, **76**, 115109.
- [61] M. Shishkin and G. Kresse, *Phys. Rev. B*, 2006, **74**, 035101.
- [62] M. Shishkin and G. Kresse, *Phys. Rev. B*, 2007, **75**, 235102.
- [63] M. Shishkin, M. Marsman and G. Kresse, *Phys. Rev. Lett.*, 2007, **99**, 246403.
- [64] P. Rinke, A. Qteish, J. Neugebauer, C. Freysoldt and M. Scheffler, *New J. Phys.*, 2005, **7**, 125.
- [65] F. Kubel and H. Schmid, *Acta Crystallogr., Sect. B: Struct. Sci.*, 1990, **B46**, 698.
- [66] A. G. Gavriliuk, V. V. Struzhkin, I. S. Lyubutin, S. G. Ovchinnikov, M. Y. Hu and P. Chow, *Phys. Rev. B*, 2008, **77**, 155112.
- [67] R. Palai, R. S. Katiyar, H. Schmid, P. Tissot, S. J. Clark, J. Robertson, S. A. T. Redfern, G. Catalan and J. F. Scott, *Phys. Rev. B*, 2008, **77**, 014110.
- [68] S. R. Basu, L. W. Martin, Y. H. Chu, M. Gajek, R. Ramesh, R. C. Rai, X. Xu and J. L. Musfeldt, *Appl. Phys. Lett.*, 2008, **92**, 091905.
- [69] A. Kumar, R. C. Rai, N. J. Podraza, S. Denev, M. Ramirez, Y. H. Chu, L. W. Martin, J. Ihlefeld, T. Heeg, J. Schubert, et al., *Appl. Phys. Lett.*, 2008, **92**, 121915.
- [70] T. Kanai, S. Ohkoshi and K. Hashimoto, *J. Phys. Chem. Solids*, 2003, **64**, 391.
- [71] F. Gao, Y. Yuan, K. F. Wang, X. Y. Chen, F. Chen and J. M. Liu, *Appl. Phys. Lett.*, 2006,

89, 102506.

- [72] T. Higuchi, Y.-S. Liu, P. Yao, P.-A. Glans, J. Guo, C. Chang, Z. Wu, W. Sakamoto, N. Itoh, T. Shimura, et al., Phys. Rev. B, 2008, **78**, 085106.
- [73] G. Henkelman, A. Arnaldsson and H. Jónsson, Comput. Mater. Sci., 2006, **36**, 254.
- [74] E. Sanville, S. D. Kenny, R. Smith and G. Henkelman, J. Comp. Chem., 2007, **28**, 899.
- [75] W. Tang, E. Sanville and G. Henkelman, J. Phys.: Condens. Matter, 2009, **21**, 084204.
- [76] P. Ravindran, R. Vidya, A. Kjekshus, H. Fjellvag and O. Eriksson, Phys. Rev. B, 2006, **74**, 224412.
- [77] F. Corà, M. Alfredsson, G. Mallia, D. S. Middlemiss, W. C. Mackrodt, R. Dovesi and R. Orlando, Struct. Bond., 2004, **113**, 171.
- [78] F. Corà, Mol. Phys., 2005, **103**, 2483.
- [79] D. Lebeugle, D. Colson, A. Forget and M. Viret, Appl. Phys. Lett., 2007, **91**, 022907.
- [80] D. J. Singh, M. Ghita, S. V. Halilov and M. Fornari, J. Phys. IV France, 2005, **128**, 47.
- [81] D. J. Singh, M. Ghita, M. Fornari and S. V. Halilov, Ferroelectrics, 2006, **338**, 73.
- [82] M. Ghita, M. Fornari, D. J. Singh and S. V. Halilov, Phys. Rev. B, 2005, **72**, 054114.
- [83] M. Suewattana and D. J. Singh, Phys. Rev. B, 2006, **73**, 224105.
- [84] K. Yamauchi, F. Freimuth, S. Bluegel and S. Picozzi, Phys. Rev. B, 2008, **78**, 014403.
- [85] J. A. Alonso, M. J. Martínez-Lopez, M. T. Casais and M. T. Fernández-Díaz, Inorg. Chem., 2000, **39**, 917.
- [86] M. W. Lufaso and P. M. Woodward, Acta Cryst. B, 2004, **60**, 10.
- [87] M. Tachibana, T. Shimoyama, H. Kawaji, T. Atake and E. Takayama-Muromachi, Phys. Rev. B, 2007, **75**, 144425.
- [88] R. L. Martin, *Electronic Structure: Basic Theory and Methods* (Cambridge University Press, 2004).
- [89] I. A. Sergienko, C.Şen and E. Dagotto, Phys. Rev. Lett., 2006, **97**, 227204.
- [90] B. Lorenz, Y.-Q. Wang and C. W. Chu, Phys. Rev. B, 2007, **76**, 104405.
- [91] V. Y. Pomjakushin, M. Kenzelmann, A. Donni, A. B. Harris, T. Nakajima, S. Mitsuda, M. Tachibana, L. Keller, J. Mesot, H. Kitazawa, et al., New J. Phys., 2009, **11**, 043019.
- [92] C. Ederer and N. A. Spaldin, Phys. Rev. B, 2005, **71**, 224103.
- [93] M. Koichi and I. Fujio, J. Appl. Cryst., 2008, **41**, 653.
- [94] J. P. Perdew, A. Ruzsinszky, G. I. Csonka, O. A. Vydrov, G. E. Scuseria, L. A. Constantin,

X. Zhou and K. Burke, Phys. Rev. Lett., 2008, **100**, 136406.

[95] I. Sosnowska, W. Schafer, W. Kockelmann, K. H. Andersen and I. O. Troyanchuk, Appl. Phys. A: Mater. Sci. Process., 2002, **74**, S1040.

[96] PBEsol[94] is a variant of the PBE exchange functional which improves equilibrium properties of densely-packed solids and their surfaces.

[97] To have an idea of the increased computational cost involved in the HSE calculation, we note that, by considering the same computational setup for BiFeO<sub>3</sub>, each electronic minimization step takes about 50 times more CPU time than PBE or PBE+U. This means that if a PBE (or PBE+U) self-consistent calculation takes 10 minutes, the HSE will take about 9 hours.

[98] Although the set of “ $t_{2g}$ ” or “ $e_g$ ” orbitals is well defined in a local coordinate frame centered on each Mn ion, this is not any more true when using the standard orthorhombic system as a global coordinate frame, due to different tilting angles and distortions on neighboring MnO<sub>6</sub> cages. Thus, our discussion for the Mn  $d$  states has only a qualitative meaning.

	PBE	B1-WC	HSE	Exp
$a_{rh}$ (Å)	5.687	5.609	5.651	5.634
$\alpha_{rh}$ (deg)	59.22	59.37	59.12	59.35
V (Å <sup>3</sup> )	127.79	122.99	125.04	124.60
$x_{Fe}$	0.223	0.219	0.219	0.221
$x_O$	0.533	0.511	0.522	0.538
$y_O$	0.936	0.926	0.931	0.933
$z_O$	0.387	0.406	0.394	0.395
$d_{Bi-O}^l$ (Å)	2.492	2.591	2.533	2.509
$d_{Bi-O}^s$ (Å)	2.308	2.196	2.249	2.270
$d_{Fe-O}^l$ (Å)	2.164	2.102	2.121	2.110
$d_{Fe-O}^s$ (Å)	1.957	1.932	1.948	1.957
$\beta_{O-Fe-O}$ (deg)	164.09	162.84	164.56	165.03
$\mu_{Fe}$ ( $\mu_B$ )	3.72	4.2	4.12	3.75
Gap (eV)	1.0	3.0	3.4	2.5-2.8

TABLE I: Dependence of structural parameters, magnetic moment and electronic band gap with respect to PBE (this work), B1-WC (Ref.[46]) and HSE (this work).  $a_{rh}$ ,  $\alpha_{rh}$ , V denote the lattice parameter, the angle, and the volume of BiFeO<sub>3</sub> in space group  $R3c$ , in the rhombohedral setting. Fe (2a) and O (6b) Wyckoff positions are also reported. Bi is in the (2a) (0,0,0) position (not reported in the table). Long (l) and short (s) bond lengths of Bi-O and Fe-O are given.  $\beta_{O-Fe-O}$  is the O-Fe-O obtuse angle (equal to 180° in the ideal octahedron).  $\mu_{Fe}$  is Fe magnetic moment. Experimental structural parameters are from Ref.[65], the experimental magnetic moment (measured on polycrystalline powder) is from Ref. [95]; the band gap is from Refs.[66–71].

BiFeO <sub>3</sub> ( <i>R3c</i> )		
BiFeO <sub>3</sub>	Q <sub>B</sub> ( <i>e</i> )	V <sub>B</sub> (Å <sup>3</sup> )
Bi	13.13 (13.01)	18.06 (17.67)
Fe	12.38 (12.13)	8.24 (7.74)
O	7.16 (7.28)	12.08 (12.38)
HoMnO <sub>3</sub> (AFM-E)		
Ho	5.18 (5.00)	7.41 (6.77)
Mn	6.82 (6.75)	12.10 (11.84)
O	7.33 (7.41)	12.42 (12.61)

TABLE II: Calculated charge and volumes according to Bader AIM partitioning for a fixed HSE geometry for BiFeO<sub>3</sub> and HoMnO<sub>3</sub>. Numbers in parenthesis are based on the HSE charge density. In all cases, we used the ferroelectric phase.

AFM-A	PBE	HSE	Exp.
Ho $4c(x, \frac{1}{4}, z)$			
$x$	0.0856	0.0859	0.0839
$z$	0.4805	0.4816	0.4825
Mn $4a(000)$			
O <sub>1</sub> $4c(x\frac{1}{4}z)$			
$x$	0.4617	0.4616	0.4622
$z$	0.6162	0.6179	0.6113
O <sub>2</sub> $8d(xyz)$			
$x$	0.3250	0.3301	0.3281
$y$	0.0550	0.0573	0.0534
$z$	0.1988	0.2018	0.2013
Mn-O (s-inpl)	1.9271	1.9022	1.9044
Mn-O (l-inpl)	2.2030	2.2393	2.2226
Mn-O (outpl)	1.9518	1.9546	1.9435
Q	0.55	0.61	0.60
$\alpha$	19.47	19.71	18.77
Mn-O-Mn (inpl)	143.849	142.839	144.081
Mn-O-Mn (outpl)	141.060	140.586	142.462

TABLE III: Structural parameters for HoMnO<sub>3</sub> optimized with AFM-A configuration in the  $Pnma$  unit cell. The lattice parameters are  $a=5.8354, b=7.3606, c=5.2572$  Å. Long and small Mn-O distances in  $c - a$  plane (inpl) and middle Mn-O distance along the  $b$  axis (outpl). Mn-O-Mn angles in the  $c - a$  plane (inpl) and interplane Mn-O-Mn angles (with apical O along the  $b$  axis).

BiFeO <sub>3</sub>	$P_{ionic}$	$P_{ele}$	$P_{tot}$	$P_{pcm}$
PBE	171.1	-65.5	105.6	87.8
HSE	177.4	-67.1	110.3	103.4
PBE(HSE)	177.4	-64.8	112.6	103.4
HSE(PBE)	171.1	-67.9	103.2	87.8
HoMnO <sub>3</sub>				
PBE	-0.6	-5.2	-5.8	-2.0
HSE	-0.3	-1.6	-1.9	-0.9
PBE(HSE)	-0.3	-3.1	-3.4	-0.9
HSE(PBE)	-0.6	-2.9	-3.5	-2.0

TABLE IV: Ferroelectric polarization of BiFeO<sub>3</sub> and HoMnO<sub>3</sub>, using PBE and HSE and Point Charge Model estimate is also given ( $P_{pcm}$ ). Units are in  $\mu C/cm^2$ . PBE (HSE) means a PBE calculation at fixed HSE geometry for the ferroelectric as well as for the paraelectric structure. Viceversa for HSE (PBE). For BiFeO<sub>3</sub> the polarization is along the [111] direction; for HoMnO<sub>3</sub> is along the  $c$  axis. The partial ionic and electronic contributions are also given. Obviously, the relative weight of ionic and electronic contributions depends on the valence electronic configuration, *e.g.* Bi  $d$  in the core or in the valence. Therefore, given an electronic configuration, we are only interested in trends of  $P_{tot}$  and  $P_{pcm}$  as far as the exchange-correlation functional is concerned.

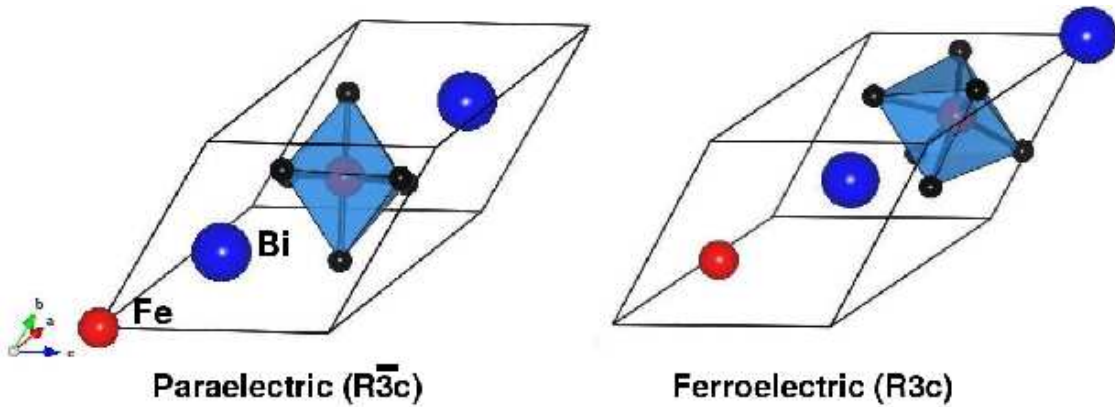


FIG. 1: (Color on line) Paraelectric  $R\bar{3}c$  and ferroelectric  $R3c$  phase of BiFeO<sub>3</sub> in the rhombohedral setting. Black spheres are oxygen atoms. The octahedron centered at one Fe atom is shown. Note the off-centering of the Fe atom and the corresponding octahedra distortion.

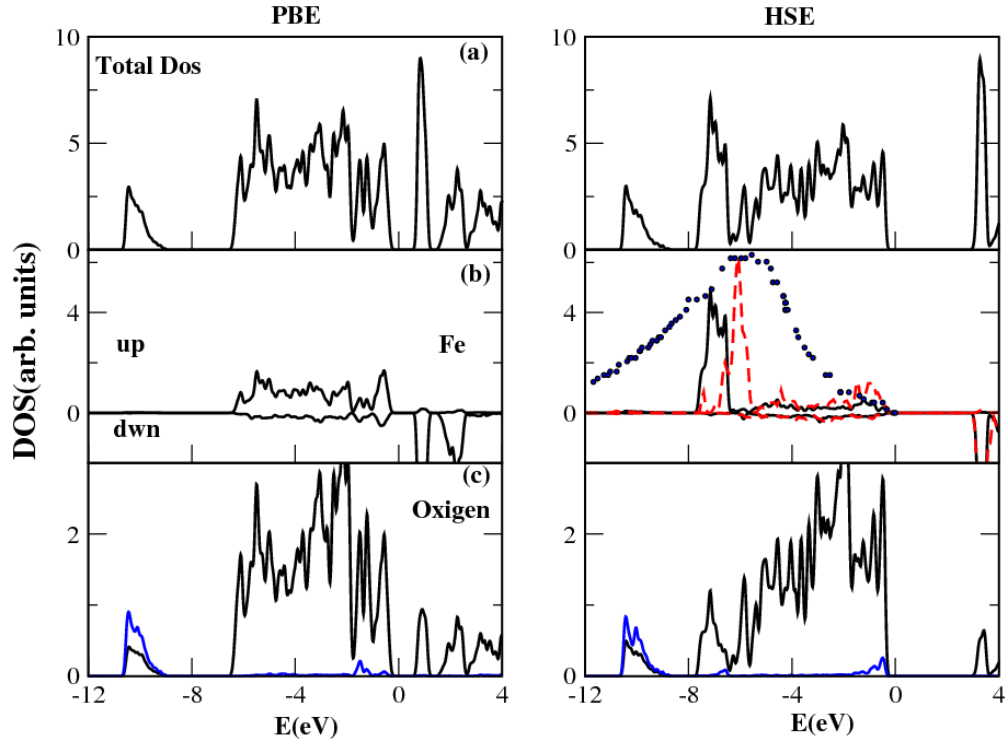


FIG. 2: (Color on line) PBE (left) and HSE (right) density of states for the ferroelectric phase of  $\text{BiFeO}_3$ . In black lines: (a) total DOS for one spin channel, (b) local Fe Dos for both spin components (minority spin are shown as negative), (c) local oxygens DOS for one spin component only. Additionally, in HSE (b), we show the Fe  $d$  DOS calculated using vertex corrections in  $W$  (see text) by red dashed line and the experimental spectral weight of  $d$  Fe taken from Ref.[72] by dotted blue lines; in (c), the magenta dashed line is Bi lone-pair DOS, *i.e.* Bi  $s$  states. The zero is set to valence band maximum.

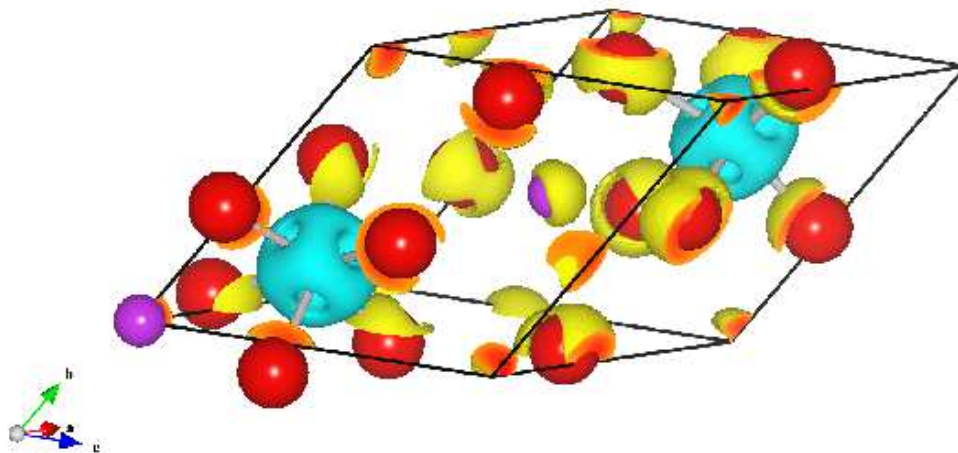


FIG. 3: (Color on line) 3D charge density difference ( $\Delta\rho = \rho^{PBE} - \rho^{HSE}$ ) isosurfaces for BiFeO3. Yellow (grey) regions correspond to an excess of HSE (PBE) charge. Only the distorted octahedron at Fe site is shown.

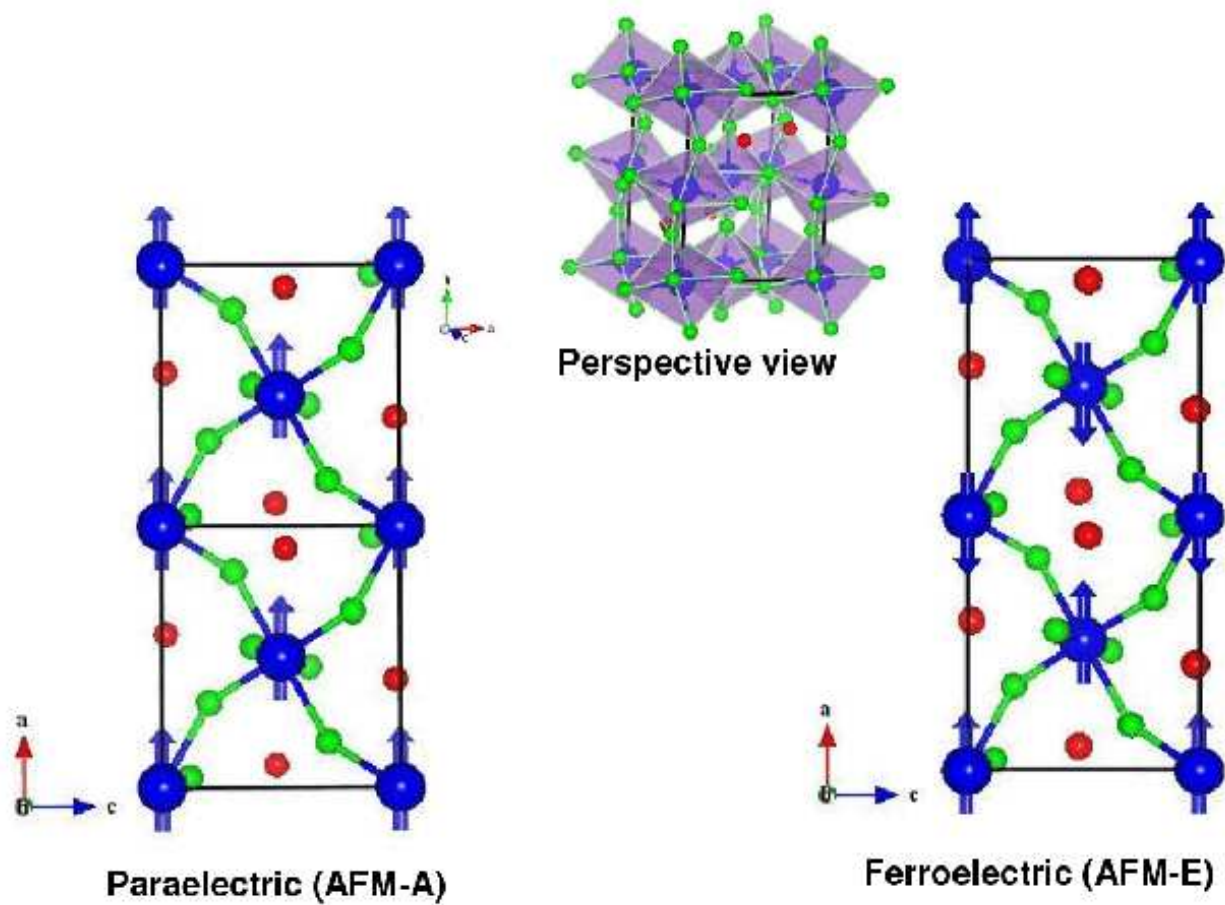


FIG. 4: (Color on line) Upper part: perspective view of  $\text{HoMnO}_3$ ; polyhedra surrounding the Mn atoms are also shown. Bottom part: paraelectric (left part) and ferroelectric (right part) spin configuration in the  $c-a$  plane. The electric polarization develops along the positive  $c$  axis. Red circles denote Ho atoms.

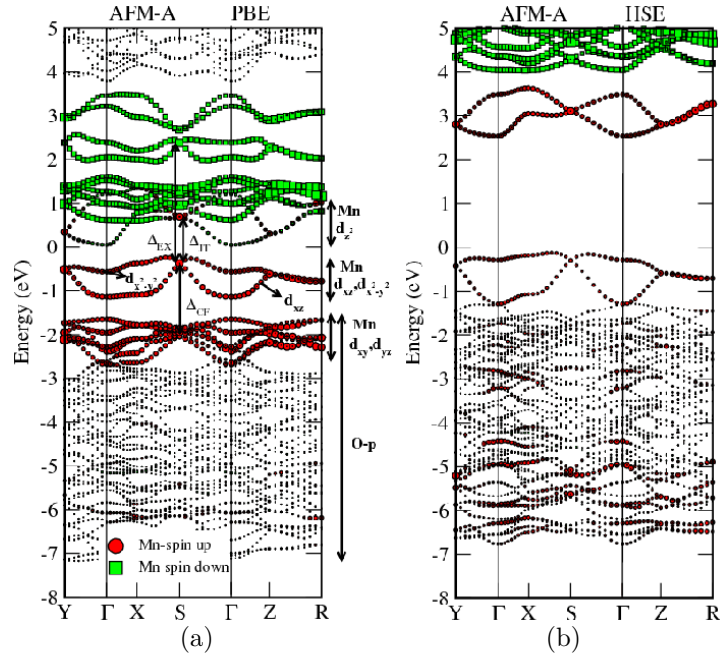


FIG. 5: (Color on line) Band structure for the AFM-A phase of  $\text{HoMnO}_3$  calculated along the symmetry lines of the orthorhombic Brillouin zone, for PBE (left) and HSE (right) using the relaxed structures. Red (green) dots refer to bands projected onto spin-up(-down) Mn atoms.

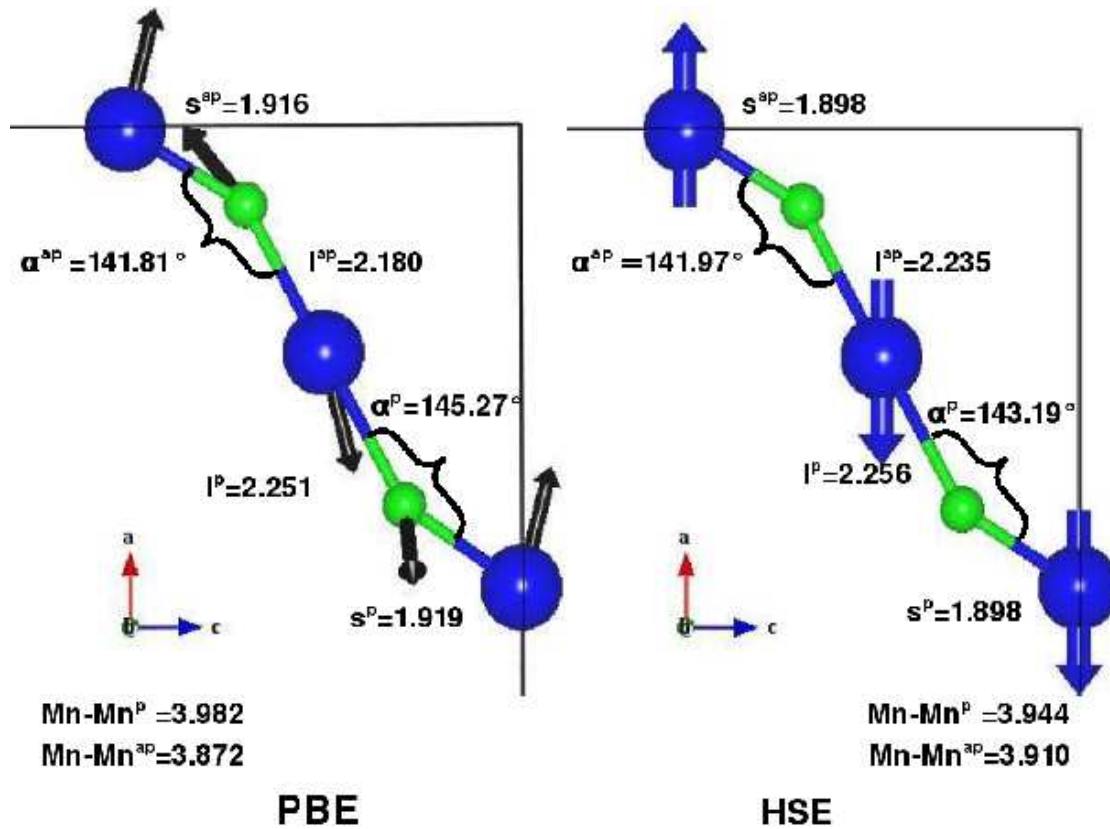


FIG. 6: (Color on line) Schematic representation of the Mn-O-Mn-O-Mn chain in the  $c - a$  plane, corresponding to the up-down-down spin configuration. The structures are in scale and all structural details are shown in the Figure (see text for further details). Distances are in Å and angles are in decimal degrees ( $^{\circ}$ ). The left (right) part corresponds to the PBE (HSE) relaxed structure. The atomic displacements projected into the  $c - a$  plane which bring the PBE structure to the HSE one are shown by black arrows (left part). The spin configuration is shown only in the HSE structure by blue arrows. Blue (green) spheres are Mn (oxygen) atoms. Ho atoms are not shown for clarity.